

# Comparison Between Thermal-Optical and L-Band Passive Microwave Soil Moisture Remote Sensing at Farm Scales: Towards UAV-Based Near-Surface Soil Moisture Mapping

Nan Ye , Jeffrey P. Walker , *Fellow, IEEE*, Ying Gao , Ivan PopStefanija , and James Hills

**Abstract**—The unmanned aerial vehicle (UAV) based remote sensing has drawn increased attention in precision agriculture. Lightweight optical and thermal sensors have been used widely on UAVs for a range of applications, and have been proposed by some as the best approach to map soil moisture at farm scales. However, passive microwave remote sensing has been widely acknowledged as the most accurate soil moisture mapping technology, and adopted by the soil moisture and ocean salinity and soil moisture active and passive satellite missions. Accordingly, it is postulated that this will also be the best technique for UAV-based near-surface soil moisture remote sensing, overcoming the spatial resolution limitation from low earth orbit altitude. Being so far limited by sensor availability, only a small number of studies have illustrated the potential of UAV-based near-surface soil moisture mapping using L-band microwave radiometers, and there has been no direct comparison with the thermal-optical alternative. To guide the design of future UAV-based soil moisture mapping systems, airborne optical, thermal infrared, and passive microwave observations collected from a scientific aircraft at low altitude over a center-pivot irrigation farm in Tasmania, Australia were used in this study to simulate UAV-based observations, and the performances of the thermal-optical and microwave techniques when compared at 75 m scale. The L-band microwave emission showed a superior sensitivity to near-surface soil moisture, and a higher and more consistent soil moisture retrieval accuracy than thermal-optical, with a root-mean-squared error of 0.05–0.06 m<sup>3</sup>/m<sup>3</sup> and 0.05–0.09 m<sup>3</sup>/m<sup>3</sup>, respectively.

**Index Terms**—Airborne field experiments, microwave, optical, remote sensing, soil moisture, thermal, unmanned aerial vehicle (UAV).

Manuscript received 9 May 2022; revised 18 January 2023, 15 May 2023, and 8 August 2023; accepted 21 October 2023. Date of publication 31 October 2023; date of current version 29 November 2023. This work was supported in part by the Tasmanian Institute of Agriculture, University of Tasmania using infrastructure funded by the Australian Research Council under Grant LE0453434 and in part by the National Natural Science Foundation of China under Grant 42071335. (*Corresponding author: Nan Ye.*)

Nan Ye, Jeffrey P. Walker, and Ying Gao are with the Department of Civil Engineering, Monash University, Clayton, VIC 3800, Australia (e-mail: ye.nan@monash.edu; jeff.walker@monash.edu; ying.gao@monash.edu).

Ivan PopStefanija is with the ProSensing Inc., Amherst, MA 01002 USA (e-mail: popstefanija@prosensing.com).

James Hills is with the Tasmanian Institute of Agriculture, University of Tasmania—Cradle Coast Campus, Burnie, TAS 7320, Australia (e-mail: james.hills@utas.edu.au).

Digital Object Identifier 10.1109/JSTARS.2023.3329015

## I. INTRODUCTION

SOIL moisture plays a key role in global water, energy, and carbon cycling [1]. Due to its high spatial and temporal variability, soil moisture distribution in space and time is required in many disciplines, especially agriculture management [2]. Over the past three decades a number of techniques have been developed for soil moisture remote sensing using visible [3], [4], thermal infrared [5], [6], passive microwave [2], [7], [8], [9], [10], active microwave [11], [12], [13], [14], [15], and their synergistic [16], [17], [18], [19], [20], [21], [22] signals. The L-band passive microwave technique has been widely acknowledged for many years as the most suitable for near-surface soil moisture mapping at regional to global scales, due to its penetration capability of the vegetation layer, independence of solar illumination, and direct relationship to soil moisture via the dielectric constant [23]. Consequently, the first two satellites dedicated to soil moisture mapping, soil moisture and ocean salinity ([24]) and soil moisture active and passive ([17]), were both based on this approach.

Unmanned aerial vehicles (UAVs) offer a small, inexpensive, and autonomous platform for soil moisture remote sensing with an improved spatial resolution and sampling flexibility compared with aircraft [25], [26], [27], [28], [29] and satellite [30], [31], [32], due to their low flying height above the ground. Moreover, recent developments in flight control systems has promoted autonomous UAV remote sensing in precision agriculture application [33], [34], [35]. A number of studies (e.g., [36], [37], [38], [39], [40]) have also illustrated the potential of light weight commercial optical and thermal sensors equipped on UAVs for surface soil moisture mapping over the whole farm with sufficient details to characterize the spatial variability. The triangle relationship [41] between land surface temperature and a vegetation index is an empirical approach, and has been the most widely used for estimating water stress and soil moisture from optical and thermal infrared data. In contrast, passive microwave sensor developments for UAV-based application have so far been limited to a few prototype research-based examples [42], [43], [44]. For example, the PoLRa radiometer with a total mass of less than 4 kg and with an antenna in the dimension of 30 cm × 60 cm × 9 mm was reported in [43]. Although L-band passive microwave remote sensing has been reported to have a

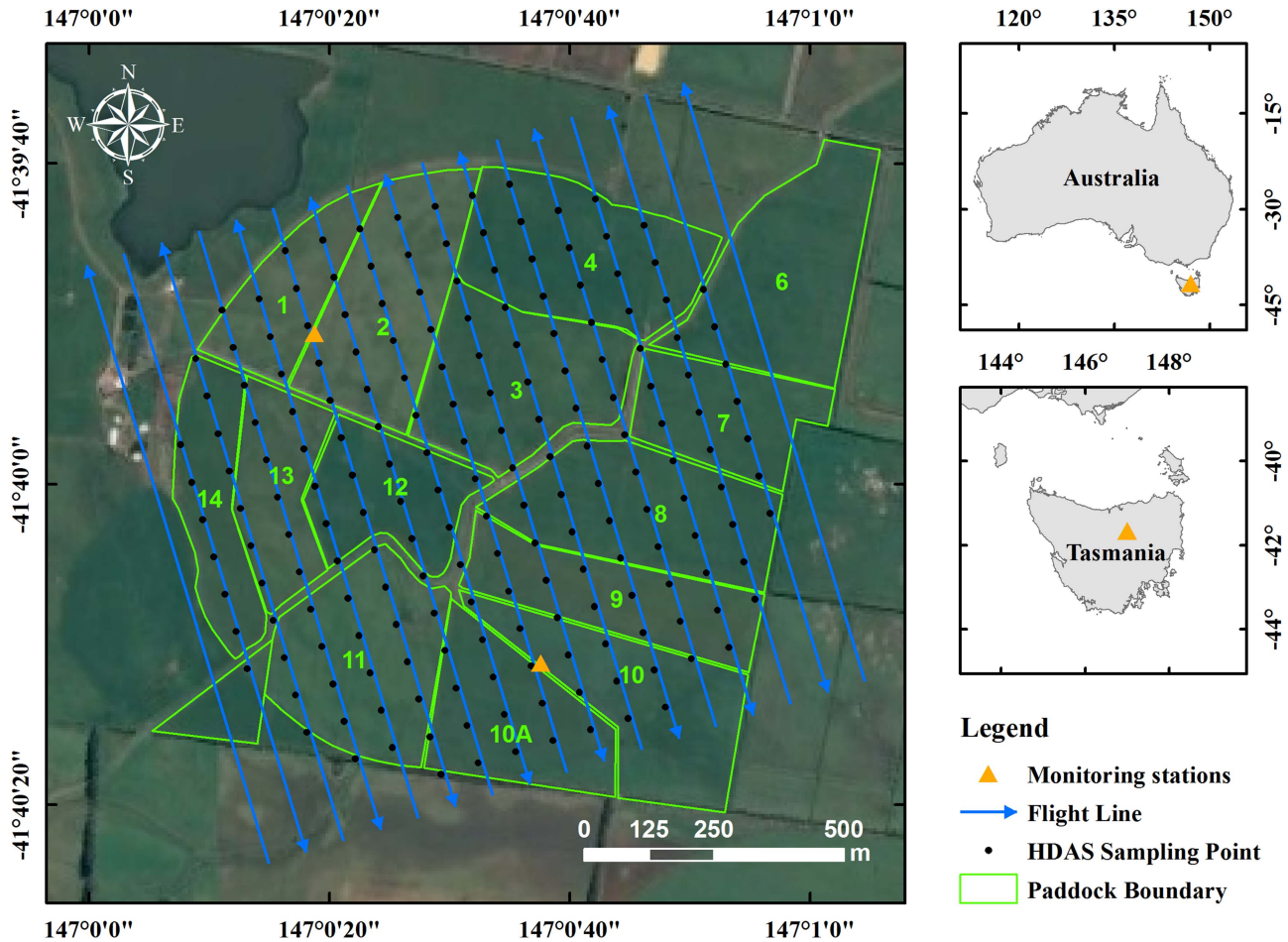


Fig. 1. Location of the study area, flight lines, monitoring stations, and ground soil moisture sampling points at Cressy, Tasmania, Australia.

higher sensitivity to soil moisture than the optical and thermal alternatives in space-borne applications [45], [46], its potential for UAV-based soil moisture mapping at high resolution and a direct comparison with the thermal-optical technique at farm scales is required to guide the design of future UAV remote sensing systems.

The objectives of this study were, therefore, to 1) simulate UAV-based multisensor data using airborne optical, thermal infrared, and passive microwave observations collected from a low altitude; 2) retrieve surface soil moisture at farm scales using a sequence of alternative algorithms; 3) evaluate the accuracy of different soil moisture retrievals using point-based ground soil moisture measurements; 4) suggest an optimal UAV configuration for soil moisture remote sensing at farm scales.

## II. MATERIALS AND METHODS

### A. Study Area

An intensive airborne field experiment was conducted over a center-pivot irrigation dairy farm at Cressy in Tasmania, Australia (see Fig. 1) between January 17th and 19th, 2017. Ye et al. [47] provided a detailed description of the experiment with a summary of pertinent details provided here. The 15 paddocks of the farm were alternately grazed and irrigated,

resulting in diverse soil moisture ( $0.10\text{--}0.66\text{ m}^3/\text{m}^3$ ) and vegetation water content ( $0.13\text{--}0.96\text{ kg}/\text{m}^2$ ) conditions, being ideal for a comparison of soil moisture remote sensing techniques. In addition, the farm was surrounded with a reservoir in the northwest and bare soil in the south, providing very wet and very dry reference points. Before the experiment, two temporary monitoring stations were installed, in Paddocks 2 and 10 A, respectively, to measure the time series of soil temperature and soil moisture profiles.

### B. Data Sets

A fixed-wing scientific aircraft was used to collect airborne observations along the designed flight lines shown in Fig. 1. Table I summarizes the technical specifications of the main instruments used in this study. Many studies (e.g., [48], [49]) have shown the potential of vegetation monitoring and normalized difference vegetation index (NDVI) mapping using commercial and modified digital cameras on UAVs. To simulate UAV-based data, the aircraft was flown at an altitude of 225 m above the ground. Accordingly, 0.2 m optical, 1.5 m thermal infrared, and 75 m L-band passive microwave observations were collected during each sampling day along 17 flight lines, together with point-based ground sampling of top 5 cm soil moisture using the

TABLE I  
SPECIFICATIONS OF THE AIRBORNE INSTRUMENTS

	Canon EOS-1Ds Mark III	Canon EOS-5Ds Mark III	FLIR A65	Polarimetric L-Band Multi-beam Radiometer (PLMR)
<b>Type:</b>	Digital Single Lens Reflex (DSLR) Camera	Digital Single Lens Reflex (DSLR) Camera	Thermal Infrared Camera	L-band microwave radiometer
<b>Dimensions (cm):</b>	15.5 x 16 x 7.9	15.2 x 11.7 x 7.6	10.7 x 4.1 x 4.3	94 x 94 x 17.8
<b>Weight (kg):</b>	1.4	1.0	0.2	43.1
<b>Frequency/Wavelength:</b>	Visible (RGB)	Visible (RG) Near Infrared (NIR)	Thermal Infrared (7.5 - 13 $\mu\text{m}$ )	Microwave (1.4 - 1.426 GHz)
<b>Observation Mode:</b>	Snap shot (5616 x 3744)	Snap shot (5760 x 3240)	Snap shot (640 x 512)	Multi-beam (linear)
<b>View angle:</b>	Nadir	Nadir	Nadir	$\pm 7^\circ$ , $\pm 21.5^\circ$ and $\pm 38.5^\circ$
<b>Beam width:</b>	$45^\circ \times 37^\circ$	$45^\circ \times 37^\circ$	$44^\circ \times 36^\circ$	$17^\circ \times 15^\circ$
<b>Spatial resolution:</b>	$\sim 0.2$ m	$\sim 0.2$ m	$\sim 1.5$ m	$\sim 75$ m

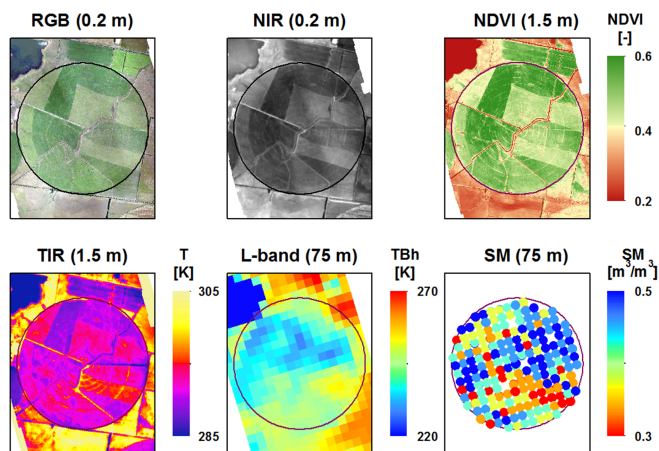


Fig. 2. Overview of airborne and ground sampling data (collected on January 19th, 2017). Airborne visible (RGB) and NIR images are plotted together with the derived NDVI map in the top row, with the airborne TIR image and L-band brightness temperature observations (at horizontal polarization with incidence angle of  $38.5^\circ$ ) plotted together with point-based ground SM measurements in the bottom row.

hydraprrobe data acquisition system (HDAS [50], [51]), which integrates a frequency domain reflectometer soil moisture sensor with a GPS and handheld computer. These sensors have been found to have an overall accuracy of  $\sim 0.04 \text{ m}^3/\text{m}^3$  under a wide range of soil moisture, soil texture, and land surface conditions. During the ground sampling, dew was not observed.

In this study, all four types of airborne observations and ground soil moisture and vegetation water content measurements were used. Fig. 2 shows an example of data collected on January 19th, 2017. Although multiangular L-band microwave brightness temperature observations were collected, only the beam with a nominal incidence angle of  $38.5^\circ$  brightness temperature observations were used here to maximize polarization difference for dual channel retrieval and to simulate the single-beam data expected from a UAV-based radiometer at L-band. As shown in Fig. 3, L-band microwave sampling flights were conducted in the early morning (7:30–8:30 A.M. local time) when the profile gradient and spatial variability of vegetation and soil temperatures was at a minimum. In contrast, thermal-optical sampling flights were conducted around noon

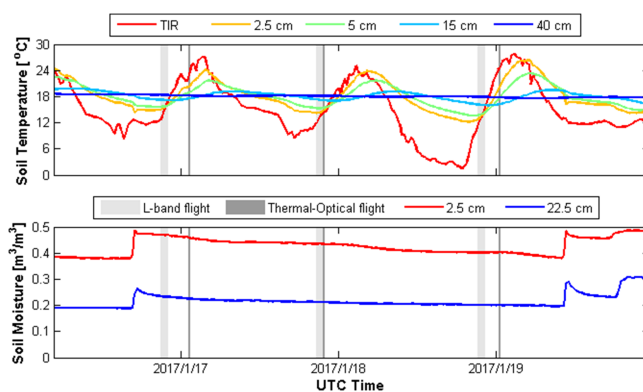


Fig. 3. Time series of TIR temperature, soil temperature at depths of 2.5 cm, 5 cm, 15 cm, and 40 cm from Paddock 10 A site (top); and time series of soil moisture at the depths of 0–5 cm, and 20–25 cm (bottom). The times of L-band and thermal-optical flights are shaded in light/dark gray.

(12:00–12:30 P.M. local time) on January 17th and 19th in order to achieve maximum temperature spatial heterogeneity and in turn thermal-optical soil moisture retrieval accuracy. To test the impact of sampling time of the day on thermal-optical soil moisture retrieval accuracy, the thermal-optical sampling flight was also carried out right after the L-band microwave sampling flight in the early morning (8:30–9:00 A.M. local time) on January 18th.

The NDVI was calculated from airborne visible (RGB) and Near InfraRed (NIR) images, as shown in the top right image of Fig. 2. The NDVI derived from the Landsat-8 OLI Red and NIR band images acquired on January 14th, 2017 was used as a reference to calibrate the airborne NDVI data. Fig. 4 shows the comparison at 30 m scale between airborne and Landsat-8 derived NDVI over each paddock and the area outside of the farm. It is clear that a good agreement was achieved for most of the paddocks (blue), while negative biases were found for the paddocks, which were grazed between January 14th and 19th, 2017 (red). Therefore, the NDVI over the ungrazed paddocks was assumed to be unchanged during the period of the experiment.

Fig. 5 shows an overview of temporal variation of thermal InfraRed (TIR) observations, L-band microwave observations, and the ground soil moisture reference measurements during the

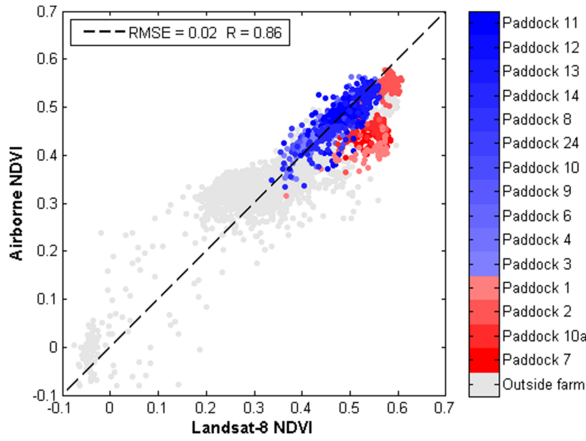


Fig. 4. Comparison between the NDVI derived from the Landsat-8 image acquired on January 14th, 2017 and the airborne visible and near infrared images collected on January 19th, 2017 over the study area.

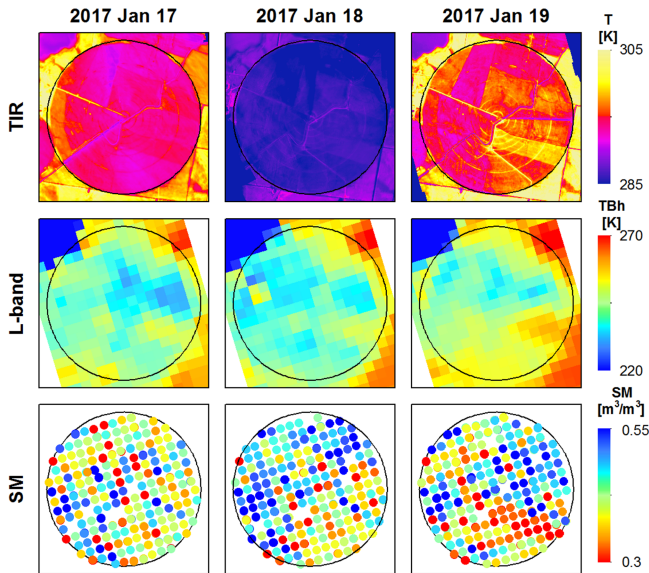


Fig. 5. Maps of TIR temperature observations (top row), L-band brightness temperature observations at horizontal polarization with an incidence angle of  $38.5^\circ$  (middle row), and point-based ground (SM; bottom row) over the study area on the three consecutive days.

period of the experiment. Since the thermal-optical flight was carried out in the morning on January 18th, 2017, the low and uniform TIR temperature confirms that the soil temperature from the monitoring stations was representative at the farm scale and could be used for estimating the effective temperature required in the passive microwave soil moisture retrieval. The multitemporal data collected from January 19th, 2017 were used to calibrate the thermal-optical and microwave soil moisture retrieval models, while data from January 17th and 18th, 2017 were used to evaluate the retrieval accuracies.

### C. Methods

1) *Thermal-Optical Soil Moisture Retrieval*: The “universal triangle” concept developed by Owen et al. [52] and further refined by Carlson [41] was used to estimate surface soil moisture

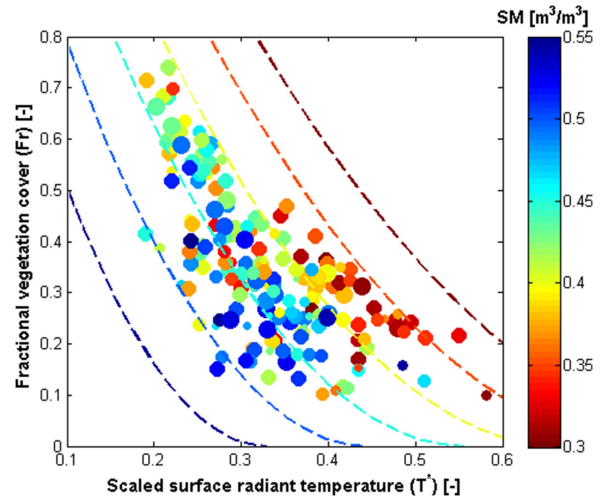


Fig. 6. Scatter plot of fractional vegetation cover ( $Fr$ ) versus surface radiant temperature ( $T^*$ ) colored by ground soil moisture, together with (1) simulated relationships for January 19th, 2017.

from the NDVI and TIR data via

$$SM = \sum_{i=0}^n \sum_{j=0}^n a_{i,j} T^{*i} Fr^j \quad (1)$$

where the subscripts  $i$  and  $j$  pertain to the surface radiant temperature  $T^*$  and the fractional vegetation cover  $Fr$ , while  $a$  indicates the coefficient for the two parameters, and  $n$  is the order of the parameters. Surface radiant temperature was normalized between the minimum and maximum TIR temperature within the study area ( $TIR_{\min}$  and  $TIR_{\max}$ , respectively), given as

$$T^* = \frac{TIR - TIR_{\min}}{TIR_{\max} - TIR_{\min}}. \quad (2)$$

Fractional vegetation cover [41] is defined as

$$Fr = \frac{NDVI - NDVI_S}{NDVI_V - NDVI_S} \quad (3)$$

where  $NDVI_S$  and  $NDVI_V$  are the NDVI of bare soil and dense vegetation, respectively; Fig. 6 shows an example scatter plot of  $Fr$  against  $T^*$  observations for January 19th, together with model simulated relationships using (1). In addition, diurnal land surface temperature change, the so called apparent thermal inertia, is strongly related to surface soil moisture [53], [54], [55]. Accordingly, Zhao and Li [56] improved (2) by replacing TIR with day-night TIR temperature difference ( $\Delta TIR$ ), given as

$$\Delta T^* = \frac{\Delta TIR - \Delta TIR_{\min}}{\Delta TIR_{\max} - \Delta TIR_{\min}} \quad (4)$$

and so (1) was updated as

$$SM = \sum_{i=0}^n \sum_{j=0}^n a_{i,j} \Delta T^{*i} Fr^j. \quad (5)$$

To also test this approach, the thermal-optical flight on January 18th carried out in the early morning was used, with the collected TIR data used as night time TIR estimates. Given

TABLE II  
DEFAULT L-MEB MODEL PARAMETERS FOR GRASSLAND, WITH THE REFERENCE TO LITERATURE PROVIDED IN BRACKETS

$HR$	$NR_h$	$NR_v$	$b$	$\omega_h$	$\omega_v$	$tt_h$	$tt_v$
0.5 [57, 58]	0 [58, 59]	0 [58, 59]	0.15 [58, 60]	0 [58]	0.05 [58]	1 [58, 59, 61]	1 [58, 59, 61]

the low and homogenous temperature distribution in the early morning, night TIR data were assumed to not change across the campaign.

2) *Microwave Soil Moisture Retrieval*: In this study, the L-MEB model [59] was used to retrieve soil moisture from dual polarized L-band brightness temperature observations at the incidence angle of  $38.5^\circ$ . Brightness temperature (TB) at polarization  $p$ , either horizontal ( $h$ ), or vertical ( $v$ ), is defined as

$$TB_p = (1 - \omega_p) \cdot (1 - \gamma_p) \cdot T_V \cdot (1 + \Gamma_p \cdot \gamma_p) + (1 - \Gamma_p) \cdot \gamma_p \cdot T_S \quad (6)$$

where  $\gamma$  is the transmissivity of the vegetation layer,  $\Gamma$  is the reflectivity of the soil surface, and  $T_V$  and  $T_S$  are the effective temperatures of the vegetation and soil layers.  $T_S$  was estimated from the top 5 cm soil moisture (SM) and the 2.5 cm ( $T_{S\_surf}$ ) and 40 cm ( $T_{S\_deep}$ ) soil temperature measurements from temporary monitoring stations via

$$T_S = T_{S\_deep} + (T_{S\_surf} - T_{S\_deep}) \cdot (SM/w_0)^{bw_0} \quad (7)$$

where the default values of parameters  $w_0 = 0.3 \text{ m}^3/\text{m}^3$  and  $bw_0 = 0.3$  [59] were used.  $T_V$  was taken as the mean of  $T_{S\_surf}$  and vegetation skin temperature from the TIR sensor. The vegetation transmissivity is a function of the vegetation optical depth at nadir ( $\tau_{NAD}$ ), the incidence angle ( $\theta$ ) and the vegetation structure coefficient ( $tt$ ) [59], given as

$$\gamma_p = \exp[-\tau_{NAD} \cdot (tt_p \cdot \sin^2(\theta) + \cos^2(\theta)) / \cos(\theta)] \quad (8)$$

with  $\tau_{NAD}$  linearly related to vegetation water content (VWC) and a coefficient  $b$  according to [60]

$$\tau_{NAD} = b \cdot \text{VWC}. \quad (9)$$

The reflectivity of the soil surface ( $\Gamma$ ) accounts for the surface roughness using parameters  $HR$  and  $NR$  via [62]

$$\Gamma_p = \Gamma_p^* \cdot \exp[-HR \cdot \cos^{NR_p}(\theta)] \quad (10)$$

where the Fresnel reflectivity of the specular surface  $\Gamma^*$  is associated with soil moisture via the soil dielectric constant, which was estimated using the Dobson model [63]. Subsequently, soil moisture retrieval and parameter calibration was undertaken using an iterative optimization approach by minimizing the cost function (CF)

$$\text{CF} = \frac{\sum (\text{TB}_{sim} - \text{TB}_{obs})^2}{\sigma(\text{TB})^2} + \sum_i \frac{\sum (P_{i,init} - P_{i,cal})^2}{\sigma(P_i)^2} \quad (11)$$

where  $\text{TB}_{sim}$  and  $\text{TB}_{obs}$  are model simulated and observed brightness temperatures. The standard deviations  $\sigma(\text{TB})$  and  $\sigma(P)$  were assigned according to the uncertainty of the brightness temperature observations and calibrated parameters, while  $P_{init}$  and  $P_{cal}$  are the initial and calibrated values of the model

parameters. The required model parameters were taken from literature [58], [59], [61], [64] and used as default values for the grassland land cover across this study area (see Table II).

#### D. Soil Moisture Retrieval

Four types of retrievals were conducted using the different configurations listed in Table III; Paddocks 6–11 in the southeast part of the farm were defined as the calibration paddocks, while the paddocks 1–4 and 12–14 were used for the validation. Accordingly, the collected data were separated into calibration and validation data. The calibration of R1 and R3 used multi-temporal data over the calibration paddocks, while R2 and R4 used data over all paddocks on January 19th, 2017 only. For the thermal-optical retrievals R1 and R2, a set of  $a_{i,j}$  was assumed to be applicable for the entire farm across the whole campaign, and calibrated using airborne TIR and NDVI data together with ground HDAS 5 cm soil moisture measurements. For the passive microwave retrievals, the roughness parameter  $HR$  in (7) was assumed to be constant throughout the campaign, and calibrated using airborne L-band brightness temperature and NDVI data together with ground soil moisture. The VWC were estimated from NDVI data via a linear relationship regressed from ground destructive vegetation sampling data, and subsequently used as inputs in the L-MEB. In R3  $HR$  was assumed to be uniform for the entire farm, while in R4  $HR$  was calibrated for each individual 75 m pixel.

### III. RESULTS AND DISCUSSION

#### A. Model Calibration

In the thermal-optical R1 and R2 retrievals a second order ( $n = 2$ ) function was used to reduce the impact of overfitting. The airborne and ground calibration observations were used to calibrate the coefficients  $a_{i,j}$ , as listed in Table IV. In the microwave R3 and R4 retrievals the parameter values in Table II were used in the L-MEB and only the  $HR$  parameter was calibrated via (10). Consequently, a  $HR$  of 1.22 was calibrated in R3, with values ranging from 0.9 to 1.9 for all 75 m pixels over the farm in R4. It can be seen from the calibrated  $HR$  in Fig. 7 that the spatial distribution of  $HR$  that correlated with the locations of paddocks, implying the requirement of paddock specific calibration. Compared with the grassland  $HR$  of 0.5 at satellite scales, it can be noted that a higher value of  $HR$  with considerable spatial variability was found at this finer scale.

#### B. Retrieved Soil Moisture

Soil moisture was subsequently retrieved from the thermal-optical and microwave observations, as shown together with ground-measured top 5 cm soil moisture in Fig. 8. It is clear that while the thermal-optical sensors had a higher spatial resolution

TABLE III  
SOIL MOISTURE RETRIEVAL CONFIGURATIONS

	Algorithm	Calibration Data	Validation Data
R1	Universal triangle	Calibration paddocks for the three days	Validation paddocks for the three days
R2	Universal triangle	All paddocks for January 19 <sup>th</sup>	All paddocks for January 17 <sup>th</sup> and 18 <sup>th</sup>
R3	L-MEB	Calibration paddocks for the three days	Validation paddocks for the three days
R4	L-MEB	All paddocks for January 19 <sup>th</sup>	All paddocks for January 17 <sup>th</sup> and 18 <sup>th</sup>

TABLE IV  
CALIBRATED COEFFICIENTS USED IN (1) FROM R1 (TOP) AND R2 (BOTTOM)

$a_{ij}$	$j = 2$	$j = 1$	$j = 0$
$i = 2$	2.962	-14.409	16.712
$i = 1$	-8.839	50.420	-57.383
$i = 0$	7.137	-39.783	41.155

$a_{ij}$	$j = 2$	$j = 1$	$j = 0$
$i = 2$	0.880	-1.377	-0.576
$i = 1$	-1.456	3.884	6.386
$i = 0$	0.290	4.250	-21.862

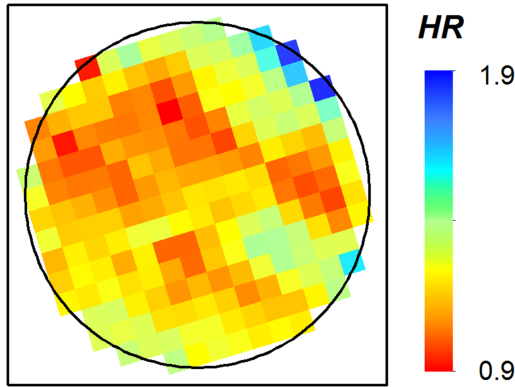


Fig. 7. Calibrated HR map from R4.

than the microwave radiometer used in this application, they were far more sensitive to sampling time of day and bore little resemblance to the ground and passive microwave derived soil moisture.

The intensive point-based 75 m spacing HDAS soil moisture measurements were interpolated on the L-band 75 m grid, but due to continuous movement of the irrigator, the location of the Centre pivot irrigator was slightly different between the airborne and ground sampling. However, the 75 m passive microwave derived soil moisture from R4 showed a similar spatial pattern to the ground soil moisture and the expected irrigation induced changes between sampling days.

### C. Evaluation

For quantitative comparison the 1.5 m resolution thermal-optical derived soil moisture data were simply arithmetically averaged to the L-band 75 m grid, based on the same assumption of uniform contribution within a 75 m pixel, as for the brightness temperature mapping process. Subsequently, thermal-optical and microwave derived soil moisture were compared with

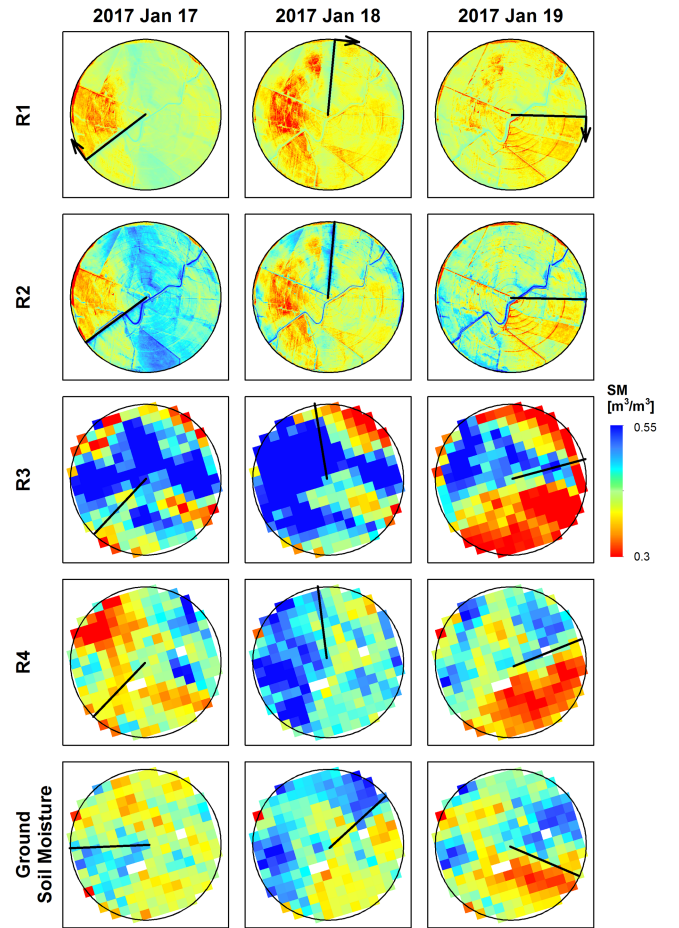


Fig. 8. Maps of the four types of airborne retrieved soil moisture (top four rows), and averaged ground top 5 cm soil moisture at 75 m scale (bottom row) over the study area on the three consecutive days. The black radiating line shows the approximate location of the centre-pivot irrigator associated with the sampling activity, and the black arrow in the top row shows the clockwise movement direction of the boom.

ground soil moisture measurements at 75 m scale, with Fig. 9 showing the scatter plots of retrieved soil moisture against ground soil moisture. Table V summarizes the performance of the four types of retrievals. It was found that R4 microwave soil moisture had lower root-mean-squared error (RMSE) and higher correlation coefficient (R) than the thermal-optical soil moisture throughout the experiment. It is noted that even on the calibration day, January 19<sup>th</sup>, 2017, the R4 microwave soil moisture had a better result than R2 thermal-optical soil moisture with an RMSE of 0.049 m<sup>3</sup>/m<sup>3</sup> and an R of 0.73, compared to 0.059 m<sup>3</sup>/m<sup>3</sup> and 0.47. In addition, statistics of the microwave soil moisture retrieval accuracy were more stable

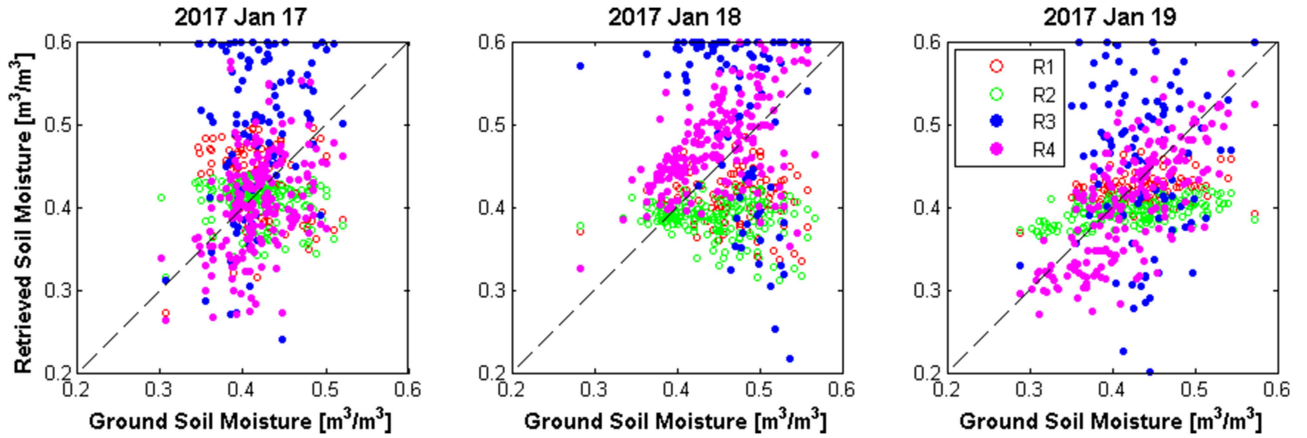


Fig. 9. Scatter plots of ground-measured soil moisture of the top 5 cm soil versus retrieved soil moisture from the four configurations using the validation data on the three consecutive days. Note that R2 and R4 did not have independent validation data on January 19th, and thus, the calibration data were shown instead.

TABLE V  
STATISTICS OF SOIL MOISTURE RETRIEVALS

Bias [ $\text{m}^3/\text{m}^3$ ] RMSE [ $\text{m}^3/\text{m}^3$ ] R [-] ubRMSE [ $\text{m}^3/\text{m}^3$ ]	Jan. 17 <sup>th</sup>	Jan. 18 <sup>th</sup>	Jan. 19 <sup>th</sup>	All Dates
<b>R1</b>	0.014 0.069 -0.17 0.068	-0.059 0.083 -0.07 0.059	-0.016 <b>0.048</b> 0.30 <b>0.045</b>	-0.020 0.068 -0.14 0.065
<b>R2</b>	<b>-0.009</b> <b>0.049</b> -0.17 <b>0.048</b>	-0.058 0.083 -0.13 0.059	-0.026 0.059 0.47 0.053	-0.031 0.065 -0.06 0.057
<b>R3</b>	0.075 0.118 0.24 0.090	0.048 0.138 -0.34 0.129	0.015 0.108 0.00 0.107	0.046 0.122 0.01 0.113
<b>R4</b>	-0.012 0.058 <b>0.39</b> 0.056	<b>0.028</b> <b>0.059</b> <b>0.50</b> <b>0.052</b>	<b>-0.014</b> 0.049 <b>0.73</b> 0.047	<b>0.001</b> <b>0.055</b> <b>0.60</b> <b>0.055</b>

The best statistics of each column was bold.

than those from the thermal-optical retrievals across different days. This confirms that from the same platform at a low altitude, microwave has a higher sensitivity to soil moisture than optical and thermal signals at farm scale.

#### D. Impact of Sampling Time of Day on Thermal-Optical Retrieval Accuracy

Since the thermal-optical observations were collected in the early morning of January 18th, 2017 when thermal infrared temperatures were relatively homogeneous and low (see top middle image of Fig. 5), the derived thermal-optical soil moisture had an opposite spatial pattern to the microwave and ground soil moisture. This might be due to thermal inertia, resulting in the dry soil having a higher temperature during day time and a lower temperature during night time than wet soil. Consequently, the temperature sequence of dry and wet soil was swapped, and so the TIR data collected on January 18th was used as the night time data in the thermal inertia based approach. Subsequently, the TIR was replaced with the TIR difference in the thermal-optical

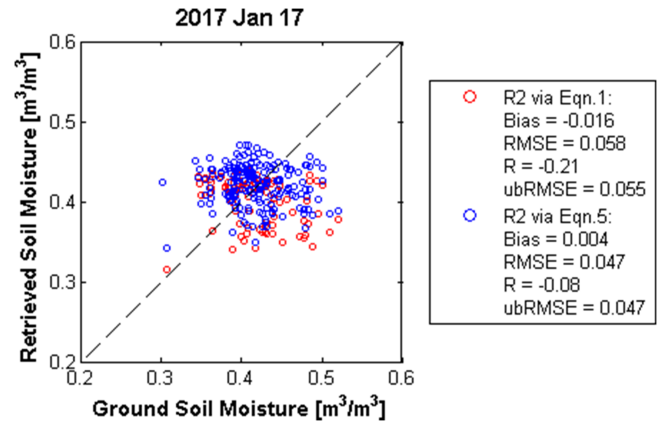


Fig. 10. Scatter plots of ground soil moisture of the top 5 cm soil versus soil moisture retrieved from the original R2 via (1) and the modified R2 via (5) using TIR differences, respectively.

method, and the R2 retrieval was repeated via (5) using data on January 19th for calibration and data on January 17th for validation. This difference in the R2 soil moisture was compared with the original R2 in Fig. 10, with a slight improvement of accuracy.

#### E. Impact of Roughness to Passive Microwave Retrieval Accuracy

The accuracy of microwave soil moisture retrieval is well understood to be affected by the  $HR$  roughness parameter. However, the retrieval accuracy in this study was found to be more sensitive to the roughness parameter  $HR$  at small scale than at the satellite scale of  $\sim 40$  km. Being different from the calibrated  $HR$  in R3, the default value used at larger scales, as shown in Table II was found to be unsuitable at small scales, inducing substantial bias in retrieved soil moisture. In addition, the improved accuracy in R4 relative to R3 implies that the spatial heterogeneity of roughness needs to be carefully considered, and thus,  $HR$  is suggested to be treated as a spatial variable at small scale.

### F. Limitations

It has been demonstrated that the microwave method had a higher overall soil moisture retrieval accuracy than the thermal-optical method. However, a few limitations need to be discussed. In this study, soil moisture measurements of the top 5 cm soil layer were used as the ground reference, which match well with the expected microwave penetration depth at L-band [17], [24], [57]. However, the optical and thermal signal is expected to mostly sense the surface of the vegetation or soil layer, and thus, a mismatch of the thermal-optical sensing depth potentially induces uncertainties to the soil moisture retrieval accuracy. In addition, the thermal-optical soil moisture retrieval method was found to be very site specific, with the correlation substantially reduced on the validation sites, limiting its application to soil wetness estimation. Conversely, the passive microwave technique is a physically based method with few semiempirical parameters related to land surface conditions. For simplification purposes, heterogeneity of topography, soil texture, and soil temperature were ignored in this study, which might have degraded the passive microwave soil moisture accuracy, but with none-the-less good results achieved. In addition, only spatial variability of the *HR* roughness parameter was considered in this study.

The evaluation and comparison of thermal-optical and passive microwave soil moisture retrievals in this study were also limited to a short period of time over a solely grass land using low altitude airborne data. However, being an irrigation farm in the summer months there was considerable spatiotemporal variation in soil moisture over that period. In addition, the study area was found to be radio frequency interference (RFI) free, which may not always be the case, and so the performance of the passive microwave remote sensing technique in RFI contaminated environments could be questionable. Furthermore, synergistic use of thermal-optical observations are expected to improve microwave soil moisture retrieval accuracy by providing higher resolution ancillary data, which can better account for spatial heterogeneity of vegetation optical depth, physical temperature, and land cover at farm scale. Consequently, to better guide the design of a UAV soil moisture remote sensing system, it is recommended that long term UAV-based soil moisture remote sensing studies be undertaken to intercompare the different technologies under more extensive land surface types and more complex electromagnetic conditions, and the combined use of thermal-optical and microwave observations be further explored.

### IV. CONCLUSION

The recent advances in UAV system capabilities provides an opportunity for high resolution soil moisture remote sensing at farm scale. While optical and thermal sensors have been used for soil moisture retrieval in many studies, the passive microwave technique at L-band has been widely acknowledged as the most promising for soil moisture remote sensing from space. However, only a few studies have used UAV-based microwave radiometers and there has been no direct farm-scale comparison of these two approaches. Accordingly, this study used low altitude airborne observations from a three-days-long field experiment

to simulate UAV-based remote sensing data over an irrigated dairy farm at Cressy in Tasmania, Australia, with thermal-optical and L-band microwave soil moisture retrieval accuracies were evaluated using intensive ground soil moisture measurements.

The “triangle method” (thermal-optical) and the L-MEB radiative transfer model (passive microwave) were used to estimate soil moisture from airborne optical, TIR, and L-band brightness temperature observations, respectively. Two approaches were applied, including data collected on January 19th, 2017 for calibration, with data from the other two days used for independent evaluation, or alternatively specific paddocks across all dates used for calibration and the others for validation. Ground point-based soil moisture measurements were compared with thermal-optical and microwave derived soil moisture at 75 m scale using a simple arithmetical average. Although the thermal-optical derived soil moisture data had a higher spatial resolution than the passive microwave soil moisture, the comparison result showed that soil moisture derived from the L-band passive microwave technique alone had a higher accuracy with better RMSE and R than thermal-optical soil moisture on both calibration and evaluation days. Moreover, the thermal-optical soil moisture retrieval algorithm is an empirical approach, which is site specific and heavily dependent on calibration using extensive ground soil moisture measurements. In contrast, the passive microwave retrieval algorithm is a physically based approach having consistent high sensitivity to soil moisture. Therefore, it has been demonstrated that the L-band radiometer outperformed the soil moisture mapping accuracy from thermal and optical cameras. It is, therefore, expected that a UAV-based microwave radiometer is the key sensor for future developments to operationalize high resolution soil moisture mapping at farm scales.

### ACKNOWLEDGMENT

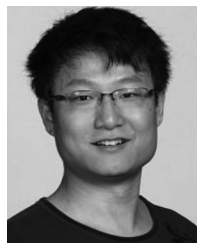
The authors would like to thank Mr. D. McLaren from the University of Tasmania and also like to thank all the experiment participants: J. Johanson, K. Mason, and J. Pudashine.

### REFERENCES

- [1] P. J. Sellers et al., “Modeling the exchanges of energy, water, and carbon between continents and the atmosphere,” *Science*, vol. 275, no. 5299, pp. 502–509, 1997.
- [2] R. A. de Jeu, T. R. Holmes, R. M. Parinussa, and M. Owe, “A spatially coherent global soil moisture product with improved temporal resolution,” *J. Hydrol.*, vol. 516, pp. 284–296, 2014.
- [3] R. Filion et al., “Remote sensing for mapping soil moisture and drainage potential in semi-arid regions: Applications to the Campidano plain of Sardinia, Italy,” *Sci. Total Environ.*, vol. 543, pp. 862–876, 2016.
- [4] N. J. Anne, A. H. Abd-Elrahman, D. B. Lewis, and N. A. Hewitt, “Modeling soil parameters using hyperspectral image reflectance in subtropical coastal wetlands,” *Int. J. Appl. Earth Observ. Geoinf.*, vol. 33, pp. 47–56, 2014.
- [5] M. Minacapilli et al., “Estimation of actual evapotranspiration of Mediterranean perennial crops by means of remote-sensing based surface energy balance models,” *Hydrol. Earth Syst. Sci.*, vol. 13, no. 7, pp. 1061–1074, 2009.
- [6] J. Qin, K. Yang, N. Lu, Y. Chen, L. Zhao, and M. Han, “Spatial upscaling of in-situ soil moisture measurements based on MODIS-derived apparent thermal inertia,” *Remote Sens. Environ.*, vol. 138, pp. 1–9, 2013.

- [7] Y. H. Kerr et al., "Overview of SMOS performance in terms of global soil moisture monitoring after six years in operation," *Remote Sens. Environ.*, vol. 180, pp. 40–63, 2016.
- [8] M. Owe, R. de Jeu, and J. Walker, "A methodology for surface soil moisture and vegetation optical depth retrieval using the microwave polarization difference index," *IEEE Trans. Geosci. Remote Sens.*, vol. 39, no. 8, pp. 1643–1654, Aug. 2001.
- [9] M. Pan, A. K. Sahoo, and E. F. Wood, "Improving soil moisture retrievals from a physically-based radiative transfer model," *Remote Sens. Environ.*, vol. 140, pp. 130–140, 2014.
- [10] N. Ye et al., "The soil moisture active passive experiments: Validation of the SMAP products in Australia," *IEEE Trans. Geosci. Remote Sens.*, vol. 59, no. 4, pp. 2922–2939, Apr. 2021.
- [11] A. Bartsch et al., "Detection of open water dynamics with ENVISAT ASAR in support of land surface modelling at high latitudes," *Biogeosciences*, vol. 9, no. 2, pp. 703–714, 2012.
- [12] R. Panciera et al., "The soil moisture active passive experiments (SMAPEx): Toward soil moisture retrieval from the SMAP mission," *IEEE Trans. Geosci. Remote Sens.*, vol. 52, no. 1, pp. 490–507, Jan. 2014.
- [13] H. Vereecken et al., "On the spatio-temporal dynamics of soil moisture at the field scale," *J. Hydrol.*, vol. 516, pp. 76–96, 2014.
- [14] L. Zhu, J. P. Walker, L. Tsang, H. Huang, N. Ye, and C. Rüdiger, "Soil moisture retrieval from time series multi-angular radar data using a dry down constraint," *Remote Sens. Environ.*, vol. 231, 2019, Art. no. 111237.
- [15] L. Zhu, J. P. Walker, L. Tsang, H. Huang, N. Ye, and C. Rüdiger, "A multi-frequency framework for soil moisture retrieval from time series radar data," *Remote Sens. Environ.*, vol. 235, 2019, Art. no. 111433.
- [16] N. N. Das et al., "The SMAP mission combined active-passive soil moisture product at 9 km and 3 km spatial resolutions," *Remote Sens. Environ.*, vol. 211, pp. 204–217, 2018.
- [17] D. Entekhabi et al., "The soil moisture active passive (SMAP) mission," *Proc. IEEE*, vol. 98, no. 5, pp. 704–716, May 2010.
- [18] Y. Y. Liu et al., "Trend-preserving blending of passive and active microwave soil moisture retrievals," *Remote Sens. Environ.*, vol. 123, pp. 280–297, 2012.
- [19] U. Narayan, V. Lakshmi, and T. J. Jackson, "High-resolution change estimation of soil moisture using L-band radiometer and radar observations made during the SMEX02 experiments," *IEEE Trans. Geosci. Remote Sens.*, vol. 44, no. 6, pp. 1545–1554, Jun. 2006.
- [20] G. Petropoulos and T. N. Carlson, "Retrievals of turbulent heat fluxes and soil moisture content by remote sensing," in *Advances in Environmental Remote Sensing: Sensors, Algorithms, and Applications*. New York, NY, USA: Taylor & Francis, 2011, pp. 469–501.
- [21] J.-P. Wigneron et al., "Modelling the passive microwave signature from land surfaces: A review of recent results and application to the L-band SMOS & SMAP soil moisture retrieval algorithms," *Remote Sens. Environ.*, vol. 192, pp. 238–262, 2017.
- [22] D. Zhang et al., "Surface soil water content estimation from thermal remote sensing based on the temporal variation of land surface temperature," *Remote Sens.*, vol. 6, no. 4, pp. 3170–3187, 2014.
- [23] F. T. Ulaby, R. K. Moore, and A. K. Fung, "Microwave remote sensing active and passive-volume I: Microwave remote sensing fundamentals and radiometry," in *Addison-Wesley Publishing Company Advanced Book Program/World Science Division*. Norwood, MA, USA: Artech House, 1981.
- [24] Y. H. Kerr et al., "The SMOS mission: New tool for monitoring key elements of the global water cycle," *Proc. IEEE*, vol. 98, no. 5, pp. 666–687, May 2010.
- [25] H. Zhang, M. Han, J. L. Chávez, and Y. Lan, "Improvement in estimation of soil water deficit by integrating airborne imagery data into a soil water balance model," *Int. J. Agricultural Biol. Eng.*, vol. 10, no. 3, pp. 37–46, 2017.
- [26] J. Bellvert, J. Marsal, J. Girona, and P. J. Zarco-Tejada, "Seasonal evolution of crop water stress index in grapevine varieties determined with high-resolution remote sensing thermal imagery," *Irrigation Sci.*, vol. 33, no. 2, pp. 81–93, 2015.
- [27] M. Gerhards et al., "Analysis of airborne optical and thermal imagery for detection of water stress symptoms," *Remote Sens.*, vol. 10, no. 7, 2018, Art. no. 1139.
- [28] H. Bai and L. Purcell, "Aerial canopy temperature differences between fast-and slow-wilting soya bean genotypes," *J. Agronomy Crop Sci.*, vol. 204, no. 3, pp. 243–251, 2018.
- [29] J. Walker et al., "High resolution soil moisture mapping," *Computing Ethics: A Multicultural Approach*. Chapman & Hall/CRC: London, UK, p. 45, 2016.
- [30] A. Calera, I. Campos, A. Osann, G. D'Urso, and M. Menenti, "Remote sensing for crop water management: From ET modelling to services for the end users," *Sensors*, vol. 17, no. 5, 2017, Art. no. 1104.
- [31] L. Du et al., "A comprehensive drought monitoring method integrating MODIS and TRMM data," *Int. J. Appl. Earth Observ. Geoinf.*, vol. 23, pp. 245–253, 2013.
- [32] D. Helman et al., "Using time series of high-resolution planet satellite images to monitor grapevine stem water potential in commercial vineyards," *Remote Sens.*, vol. 10, no. 10, 2018, Art. no. 1615.
- [33] O. Vergara-Díaz et al., "A novel remote sensing approach for prediction of maize yield under different conditions of nitrogen fertilization," *Front. Plant Sci.*, vol. 7, p. 666, 2016.
- [34] P. J. Zarco-Tejada, J. A. Berni, L. Suárez, G. Sepulcre-Cantó, F. Morales, and J. R. Miller, "Imaging chlorophyll fluorescence with an airborne narrow-band multispectral camera for vegetation stress detection," *Remote Sens. Environ.*, vol. 113, no. 6, pp. 1262–1275, 2009.
- [35] P. J. Zarco-Tejada, M. L. Guillén-Climent, R. Hernández-Clemente, A. Catalina, M. González, and P. Martín, "Estimating leaf carotenoid content in vineyards using high resolution hyperspectral imagery acquired from an unmanned aerial vehicle (UAV)," *Agricultural Forest Meteorol.*, vol. 171, pp. 281–294, 2013.
- [36] L. Hassan-Esfahani, A. Torres-Rua, A. M. Tielavilca, A. Jensen, and M. McKee, "Topsoil moisture estimation for precision agriculture using unmanned aerial vehicle multispectral imagery," in *Proc. IEEE Geosci. Remote Sens. Symp.*, 2014, pp. 3263–3266.
- [37] H. Hoffmann, R. Jensen, A. Thomsen, H. Nieto, J. Rasmussen, and T. Friberg, "Crop water stress maps for an entire growing season from visible and thermal UAV imagery," *Biogeosciences*, vol. 13, no. 24, pp. 6545–6563, 2016.
- [38] D. Turner, A. Lucieer, and C. Watson, "Development of an unmanned aerial vehicle (UAV) for hyper resolution vineyard mapping based on visible, multispectral, and thermal imagery," in *Proc. 34th Int. Symp. Remote Sens. Environ.*, 2011, p. 4.
- [39] F. Lu, Y. Sun, and F. Hou, "Using UAV visible images to estimate the soil moisture of steppe," *Water*, vol. 12, no. 9, 2020, Art. no. 2334.
- [40] E. Babaeian, S. Paheding, N. Siddique, V. K. Devabhaktuni, and M. Tuller, "Estimation of root zone soil moisture from ground and remotely sensed soil information with multisensor data fusion and automated machine learning," *Remote Sens. Environ.*, vol. 260, 2021, Art. no. 112434.
- [41] T. Carlson, "An overview of the 'triangle method' for estimating surface evapotranspiration and soil moisture from satellite imagery," *Sensors*, vol. 7, no. 8, pp. 1612–1629, 2007.
- [42] R. Acevo-Herrera et al., "Design and first results of an UAV-borne L-band radiometer for multiple monitoring purposes," *Remote Sens.*, vol. 2, no. 7, pp. 1662–1679, 2010.
- [43] D. Houtz, R. Naderpour, and M. Schwank, "Portable L-band radiometer (PoLRa): Design and characterization," *Remote Sens.*, vol. 12, no. 17, 2020, Art. no. 2780.
- [44] E. Dai, A. Gasiewski, A. Venkatasubramony, M. Stachura, and J. Elston, "L-band soil moisture mapping using a small unmanned aerial system," in *Proc. IEEE Int. Geosci. Remote Sens. Symp.*, 2017, pp. 2031–2034.
- [45] D. Zhang and G. Zhou, "Estimation of soil moisture from optical and thermal remote sensing: A review," *Sensors*, vol. 16, no. 8, 2016, Art. no. 1308.
- [46] L. Wang and J. J. Qu, "Satellite remote sensing applications for surface soil moisture monitoring: A review," *Front. Earth Sci. China*, vol. 3, no. 2, pp. 237–247, 2009.
- [47] N. Ye et al., "Toward P-band passive microwave sensing of soil moisture," *IEEE Geosci. Remote Sens. Lett.*, vol. 18, no. 3, pp. 504–508, Mar. 2021.
- [48] E. F. Berra, R. Gaulton, and S. Barr, "Commercial off-the-shelf digital cameras on unmanned aerial vehicles for multitemporal monitoring of vegetation reflectance and NDVI," *IEEE Trans. Geosci. Remote Sens.*, vol. 55, no. 9, pp. 4878–4886, Sep. 2017.
- [49] F. H. Holman, A. B. Riche, M. Castle, M. J. Wooster, and M. J. Hawkesford, "Radiometric calibration of 'commercial off the shelf' cameras for UAV-based high-resolution temporal crop phenotyping of reflectance and NDVI," *Remote Sens.*, vol. 11, no. 14, 2019, Art. no. 1657.
- [50] R. Panciera, O. Merlin, R. Young, and J. Walker, *The Hydraprobe Data Acquisition System (HDAS): User Guide*. Melbourne, Australia: Univ. Melbourne, Report, 2006.
- [51] O. Merlin, J. P. Walker, R. Panciera, R. Young, J. D. Kalma, and E. J. Kim, "Calibration of a soil moisture sensor in heterogeneous terrain," in *Proc. MODSIM Int. Congr. Modelling Simul.*, Modelling and Simulation Society of Australia and New Zealand, pp. 2604–2610, 2007.

- [52] T. Owen, T. Carlson, and R. Gillies, "An assessment of satellite remotely-sensed land cover parameters in quantitatively describing the climatic effect of urbanization," *Int. J. Remote Sens.*, vol. 19, no. 9, pp. 1663–1681, 1998.
- [53] B. Fang, V. Lakshmi, R. Bindlish, T. J. Jackson, M. Cosh, and J. Basara, "Passive microwave soil moisture downscaling using vegetation index and skin surface temperature," *Vadose Zone J.*, vol. 12, no. 3, 2013, Art. no. vzt2013.
- [54] M. Minacapilli, C. Cammalleri, G. Ciraolo, F. D'Asaro, M. Iovino, and A. Maltese, "Thermal inertia modeling for soil surface water content estimation: A laboratory experiment," *Soil Sci. Soc. Amer. J.*, vol. 76, no. 1, pp. 92–100, 2012.
- [55] F. Veroustraete et al., "Soil moisture content retrieval based on apparent thermal inertia for Xinjiang province in China," *Int. J. Remote Sens.*, vol. 33, no. 12, pp. 3870–3885, 2012.
- [56] W. Zhao and A. Li, "A comparison study on empirical microwave soil moisture downscaling methods based on the integration of microwave-optical/IR data on the Tibetan Plateau," *Int. J. Remote Sens.*, vol. 36, no. 19/20, pp. 4986–5002, 2015.
- [57] X. Shen et al., "Soil moisture retrieval depth of P-and L-band radiometry: Predictions and observations," *IEEE Trans. Geosci. Remote Sens.*, vol. 59, no. 8, pp. 6814–6822, Aug. 2021.
- [58] R. Panciera, J. P. Walker, J. D. Kalma, E. J. Kim, K. Saleh, and J.-P. Wigneron, "Evaluation of the SMOS L-MEB passive microwave soil moisture retrieval algorithm," *Remote Sens. Environ.*, vol. 113, no. 2, pp. 435–444, 2009.
- [59] J.-P. Wigneron et al., "L-band microwave emission of the biosphere (L-MEB) model: Description and calibration against experimental data sets over crop fields," *Remote Sens. Environ.*, vol. 107, no. 4, pp. 639–655, 2007.
- [60] T. J. Jackson and T. J. Schmugge, "Vegetation effects on the microwave emission of soils," *Remote Sens. Environ.*, vol. 36, no. 3, pp. 203–212, 1991.
- [61] J. P. Grant et al., "Calibration of the L-MEB model over a coniferous and a deciduous forest," *IEEE Trans. Geosci. Remote Sens.*, vol. 46, no. 3, pp. 808–818, Mar. 2008.
- [62] T. Mo and T. J. Schmugge, "A parameterization of the effect of surface roughness on microwave emission," *IEEE Trans. Geosci. Remote Sens.*, vol. GE-25, no. 4, pp. 481–486, Jul. 1987.
- [63] M. C. Dobson, F. T. Ulaby, M. T. Hallikainen, and M. A. El-Rayes, "Microwave dielectric behavior of wet soil-Part II: Dielectric mixing models," *IEEE Trans. Geosci. Remote Sens.*, vol. GE-23, no. 1, pp. 35–46, Jan. 1985.
- [64] R. Panciera et al., "The NAFE'05/CoSMOS data set: Toward SMOS soil moisture retrieval, downscaling, and assimilation," *IEEE Trans. Geosci. Remote Sens.*, vol. 46, no. 3, pp. 736–745, Mar. 2008.



**Nan Ye** received the B.E. degree in hydraulic and hydropower engineering from Tsinghua University, Beijing, China, in 2006, and the Ph.D. degree in civil engineering from Monash University, Melbourne, VIC, Australia, in 2014.

He coordinated a number of airborne field experiments for the in-orbit calibration/validation of the Soil Moisture Active Passive mission in the Murrumbidgee River catchment, southeast of Australia. He is currently an Adjunct Research Fellow with Monash University working on P-band passive microwave remote sensing of soil moisture.



**Jeffrey P. Walker** (Fellow, IEEE) received the B.E. (civil) and B.Surveying degrees in 1995 (with hon. 1 and University Medal) and the Ph.D. degree in water resources engineering in 1999 from the University of Newcastle, Callaghan, NSW, Australia.

His Ph.D. thesis was among the early pioneering research on estimation of root-zone soil moisture from assimilation of remotely sensed surface soil moisture observations. He was with the NASA Goddard Space Flight Centre to implement his soil moisture work globally. In 2001, he was with the Department of Civil and Environmental Engineering, University of Melbourne as Lecturer, where he continued his soil moisture work, including development of the only Australian airborne capability for simulating new satellite missions for soil moisture. In 2010, he was a Professor with the Department of Civil Engineering, Monash University, where he is continuing this research. He is contributing to soil moisture satellite missions at NASA, ESA, and JAXA, as a Science Team member for the Soil Moisture Active Passive mission and Cal/val Team member for the Soil Moisture and Ocean Salinity and Global Change Observation Mission – Water, respectively.



**Ying Gao** received the B.E. degree (hons. 1) from Monash University, Melbourne, VIC, Australia, and from Central South University, Changsha, China, in 2010, and the Ph.D. degree from Monash University, in 2016, all in civil engineering.

Since 2016, she has been with Monash University as a Research Fellow. Her research interests include active and passive microwave remote sensing, optical sensing of vegetation, and surface roughness parameterization.

**Ivan PopStefanija** biography is not available at the time of publication.

**James Hills** biography is not available at the time of publication.